

Time-resolved electric probe techniques in radio frequency plasmas

D. N. Ruzic and Jeffrey L. Wilson

Citation: *J. Vac. Sci. Technol. A* **8**, 3746 (1990); doi: 10.1116/1.576488

View online: <http://dx.doi.org/10.1116/1.576488>

View Table of Contents: <http://avspublications.org/resource/1/JVTAD6/v8/i5>

Published by the AVS: Science & Technology of Materials, Interfaces, and Processing

Related Articles

Can surface cracks and unipolar arcs explain breakdown and gradient limits?

J. Vac. Sci. Technol. A **31**, 011302 (2013)

Mechanically robust silica-like coatings deposited by microwave plasmas for barrier applications

J. Vac. Sci. Technol. A **30**, 061502 (2012)

Spatially resolved measurements of ion density and electron temperature in a dual-frequency capacitively coupled plasma by complete floating double probe technique

J. Vac. Sci. Technol. A **29**, 011006 (2011)

High etching rates of bulk Nb in Ar/Cl₂ microwave discharge

J. Vac. Sci. Technol. A **27**, 301 (2009)

Study of fluorocarbon plasma in 60 and 100MHz capacitively coupled discharges using mass spectrometry

J. Vac. Sci. Technol. A **26**, 1198 (2008)

Additional information on *J. Vac. Sci. Technol. A*

Journal Homepage: <http://avspublications.org/jvsta>

Journal Information: http://avspublications.org/jvsta/about/about_the_journal


Top downloads: http://avspublications.org/jvsta/top_20_most_downloaded

Information for Authors: http://avspublications.org/jvsta/authors/information_for_contributors

ADVERTISEMENT


Instruments for advanced science

Gas Analysis




- dynamic measurement of reaction gas streams
- catalysis and thermal analysis
- molecular beam studies
- dissolved species probes
- fermentation, environmental and ecological studies

Surface Science




- UHV TPD
- SIMS
- end point detection in ion beam etch
- elemental imaging - surface mapping

Plasma Diagnostics



- plasma source characterization
- etch and deposition process reaction kinetic studies
- analysis of neutral and radical species

Vacuum Analysis



- partial pressure measurement and control of process gases
- reactive sputter process control
- vacuum diagnostics
- vacuum coating process monitoring

contact Hiden Analytical for further details

HIDEN ANALYTICAL

info@hideninc.com
www.HidenAnalytical.com
CLICK to view our product catalogue

Time-resolved electric probe techniques in radio frequency plasmas

D. N. Ruzic and Jeffrey L. Wilson

Department of Nuclear Engineering, University of Illinois, Urbana, Illinois 61801

(Received 7 February 1990; accepted 12 May 1990)

Time-resolved cross-sectional variation of plasma potential and electron energies were measured in a parallel-plate capacitively coupled argon discharge at 400 mTorr. Movable capacitive and shielded Langmuir probes were scanned between the plates and used to obtain I - V characteristics at the plasma potential minima and maxima. The variation of plasma potential was sinusoidal at the center of the discharge producing a sheath at both electrodes. During the plasma potential minima and maxima an electron beam component of the electron energy distribution at 5–26 eV was seen. The energy of the beam increased, and its magnitude decreased, traversing through the sheath region. Electron beam energy variations with pressure (200 mTorr–1 Torr) are also discussed.

I. INTRODUCTION

Plasma processing is the production of ions and/or neutral radicals which act upon a surface in some manner. Plasma processing has become the dominant tool of semiconductor manufacturing enabling a high degree of anisotropy which, in turn, has reduced the feature size on integrated circuits to less than 1μ . These surface reactions can (1) allow the semiconductor surface itself to be etched as in reactive ion etching, (2) erode a separate target which then coats the semiconductor surface as in magnetron sputtering, or (3) grow a film directly on top of the semiconductor as in glow-discharge deposition. A comprehensive review of all these plasma based processes has recently been published.¹

The understanding of the plasmas in these devices is in its infancy. In many cases the identity of the species that arrive at the surface is unknown. Since direct measurement of the neutral radical species is quite difficult, or even impossible, under the conditions where there is a fine line between producing high quality integrated circuits and ones of less utility, modeling efforts are called for.

To predict the species that will arrive on a surface from the plasma interactions that create the radicals, the electron energy distribution in the plasma as a function of position and time must be known. The cross sections for most electron-impact induced molecular dissociations and ionizations have a very sharp cutoff near 10 eV.² Typically the bulk of the electrons in plasma devices have an average energy below this level. Therefore, the energetic electrons in the tail of the distribution drive the plasma chemistry. Since the electrons' plasma frequency is typically much higher (gigahertz range) than the radio frequency (rf) driving frequency (13.56 MHz), the electrons will react to the rf. The number and energy of the electrons will vary over the rf cycle and vary with position in the device. The electron energy distribution will not be Maxwellian at the higher energies where there is a significant cross section for many of the ionization and dissociation processes. In this paper direct measurements of time and space resolved electron energy distributions are presented as a first step toward resolving the detailed plasma interactions.

Knowledge of the identity and relative number of the arriving species is still not enough to determine the surface interactions. The energy of the arriving ions is an important factor in controlling the rate of surface free-bond formation and/or damage to the lattice structure. Since ions are accelerated by the plasma sheaths at the material boundaries, the plasma potential as a function of position and time must also be known to determine the energy distribution of the arriving flux. In this paper the plasma potential variation across a discharge at two times—the time of maximum plasma potential and the time of minimum plasma potential is also reported.

These measurements have been performed in a commercial parallel-plate plasma etching device with an Ar plasma. While molecular and reactive gases will differ in many respects from Ar discharges, the electrons will react to rf electric fields in a similar manner. Therefore the electron energy distribution and plasma potential variation with space and time may have direct relevance to typical processing plasmas.

II. EXPERIMENTAL

Figure 1 shows a schematic arrangement of the experimental set up. The capacitively coupled parallel plate plasma chamber, Davis and Wilder model no. 425, had a diameter of 70.1 cm and an electrode spacing of 3.7 cm. Both electrodes were water cooled. The bottom electrode was grounded. Quartz plates lie above the top, powered, electrode and radially along the inside cylindrical wall to separate the walls of the chamber from the plasma. Vacuum was maintained by a DuoSeal model no. 1397 roughing pump and a Liebold-Heraeus model no. WAU20 roots blower. Ultimate pressure of the chamber as measured by a MKS Baratron model no. 122A with a 1 Torr head was less than 5 mTorr. The data presented here was obtained from a 400 ± 5 mTorr argon plasma.

A Tegal 300 W 13.56 MHz generator supplied rf power through an associated Tegal matching network. Power was monitored by a Bird rf directional "thru-line" wattmeter,

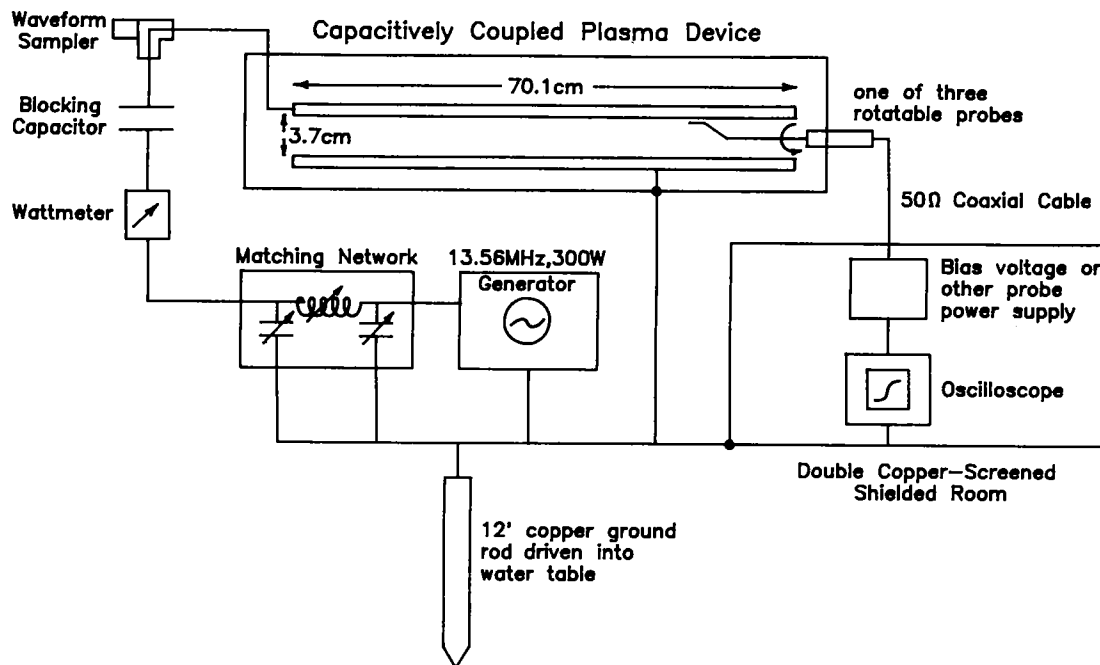


FIG. 1. Schematic of the experimental apparatus showing the single point ground paths used to eliminate ground loops.

model no. 4342 and the waveform sampled by a capacitively coupled Bird waveform sampler. A blocking capacitor was positioned between the wattmeter and the waveform sampler. Power was maintained at 100 ± 5 W forward and 40 ± 2 W reflected.

Measurements of the plasma parameters were taken within a double-shielded copper-screen room. This shield room was essential to the reduction of unwanted rf interference broadcast from the supply and other sources. Without the shield room, noise was picked up at the connections to the probe power supplies and measuring devices. The 120 V alternate current (ac) power supplied to these instruments within the room was fed through a low pass filter. The rf generator, rf matching network, grounded electrode, chamber chassis, screen room, and vacuum pumps were all grounded to a single point directly beneath the plasma chamber eliminating all ground loops. The ground point was established by driving a 3 m long, 2 cm diam copper rod through the floor of the building into the water table.

Three double-shielded electric probes were inserted into the plasma chamber through the side walls. These probes are 50 Ω coaxial cables whose center conductor is spot welded to a 0.4 mm diam W tip. A stainless steel tube provides the second layer of shielding and a ceramic coating over the tube avoids shorting the plasma. One of the three probes had the probe tip covered with the ceramic layer as well, thus acting as a capacitive probe. All of the probes could rotate and thus sweep the plasma from plate to plate as shown in Fig. 1.

The capacitive probe was connected to a high-input impedance FET rf preamplifier circuit. It measured the time-

varying ac floating potential. One of the exposed probes was connected directly to the 10^6 - Ω input of the scope and measured the dc floating potential. The other exposed probe was terminated on 50 Ω and functioned as a Langmuir probe. To obtain time-resolved Langmuir probe traces, the 13.56 MHz signal from the Langmuir probe was monitored as a function of bias voltage applied to the probe. The maxima of the rf signal corresponds to the current obtained at the time of minimum plasma potential. The minima of the rf signal corresponds to the current obtained at the maximum plasma potential. More details of the probe construction, circuitry and measurement technique are described elsewhere.³⁻⁵

In any electric probe measurements there are many problems associated with the acquisition and interpretation of the data. The foremost of these problems is that the presence of the probe disturbs the plasma being measured. In this experiment the extent of the plasma disturbance was quantified by moving a second probe of identical construction next to the first probe while taking data. There was no discernable effect on the probe signal when the second probe was brought within 5 mm.

To quantify electron energies, the ion current must be subtracted from the total probe current in a consistent manner. Ion current is proportional to the square root of the plasma potential minus the bias voltage.⁶ A linear subtraction of ion current can only be applied if the magnitude of the ion current is much less than the electron current. In this experiment, a linear subtraction of the ion current was employed since the magnitude of the ion current even in the ion saturation region was less than 10% of the electron current at the

first sharp rise (see Sec. III) of the probe signal.

To quantify densities, the effective probe area must be considered and not just the geometric area of the probe tip. One of the most useful analysis techniques in this regime where the dimensions of the probe are comparable with the mean-free path of the electrons, is the Laframboise method of successive approximations.⁷ Only a rough estimate of the electron density was obtained from the ion saturation current in this work, $1.0 \pm 0.7 \times 10^9 \text{ cm}^{-3}$.

When a current or voltage is obtained from an electric probe, a correction must be added to account for the loadline of the measuring device. Only a probe with an infinite impedance truly reads the floating potential of a plasma. Only a probe with zero impedance reads the current.⁸ In this work these load-line corrections were not applied to the measured currents and voltages since the correction factors were smaller than other sources of uncertainty in the data.

When reading a rf signal at the same frequency as the rf generator extreme care must be taken to ensure that the signal is coming from the plasma itself and not transmitted noise. All ground loops must be eliminated and the measurement devices must be isolated. Calibration must be done as a function of frequency and the same geometry, cable lengths, relative placement of the instruments etc. must be maintained. The calibration of rf signals is dependent on stray capacitance to ground and the capacitance of the cables. The calibrations for this work used the identical set up as the measurements. For the capacitive probe, the conducting plasma was simulated by immersing the probe tips into small pools of Hg.⁹

Despite all of these corrections, the resultant electron current versus bias voltage ($I-V$) curve cannot be analyzed assuming a Maxwellian distribution of electrons in the plasma. Parallel plate discharges contain energetic secondary electrons produced by the impact of the ions with the plates which are then accelerated by the sheath. Stochastic sheath heating of the electrons largely sustains the level of ionization in the discharge.¹⁰ If time-resolved $I-V$ curves are not used, the presence of the accelerated electrons will be missed. If a Maxwellian analysis is applied to determine some measure of average bulk electron energy, a "temperature" of $4.0 \pm 1.0 \text{ eV}$ is found.

Figure 2 shows three possible $I-V$ curves that could result from discharges with energetic particles.¹¹ The first trace shows the presence of an electron beam. These electrons have energy E_{eb} and are not repelled from the probe until the bias potential reaches $V_p - (E_{eb}/e)$. The second trace shows an $I-V$ curve with energetic electrons which are not uniformly directed toward the probe surface. As the number of collisions increase a beam-type behavior of Fig. 2(a) may degrade into the $I-V$ curve shown in Fig. 2(b).

There is a danger in interpreting a two-knee $I-V$ curve as an electron beam and plasma potential. Figure 2(c) shows a two-knee distribution where the first sharp rise occurs at plasma potential and the second rise is due either to an ion beam of energy E_{ib} or enhanced ionization around the probe tip giving rise to an additional current ΔI_b . In the case of enhanced ionization, the distance between the two knees is the ionization potential of the gas V_I .

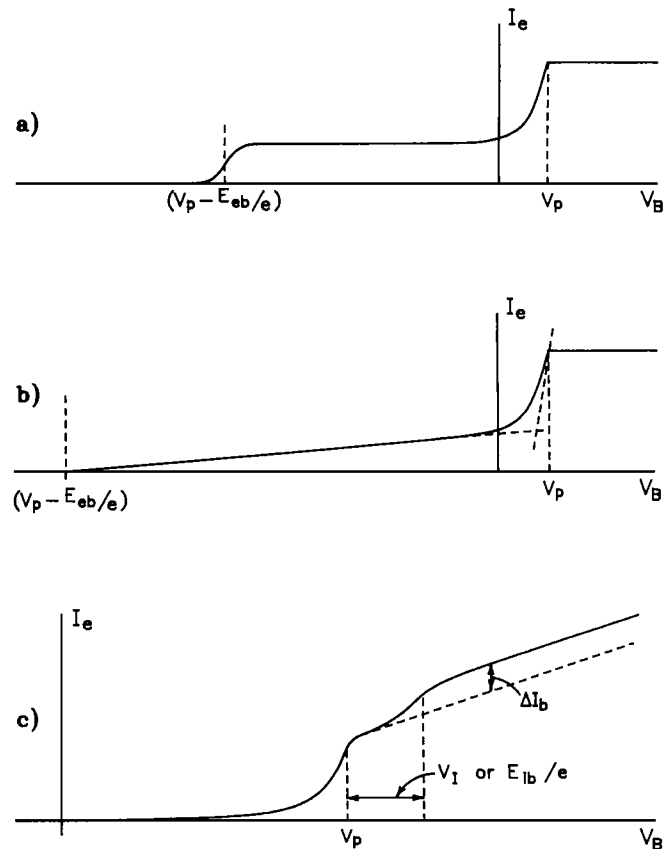


FIG. 2. Possible forms¹¹ of instantaneous electron current (I_e) vs bias voltage at the probe tip (V_b) for (a) a plasma with an electron beam directed toward the probe tip with energy E_{eb} , (b) a plasma with an energetic electron component of energy E_{eb} , (c) a plasma with an energetic ion beam of energy E_{ib} or a plasma with ionization potential V_I showing enhanced ionization near the probe tip. V_p is the plasma potential.

III. RESULTS

The time-varying floating potential was sinusoidal at all measured positions. The peak-to-peak magnitude of the ac floating potential obtained from the calibrated capacitive probe is shown in Fig. 3(a) as a function of position. The standard deviation in the measured values was $\pm 0.3 \text{ V}$. Distances between the parallel plates are measured from the grounded electrode (0 mm) to the powered electrode (37 mm). Figure 3(b) shows the dc floating potential as a function of position across the discharge obtained from the high-input impedance electric probe. The standard deviation in the measured values was $\pm 0.1 \text{ V}$. These measurements can be combined to obtain the total floating potential as a function of position and time. Figure 3(c) shows the detailed positional variation of the maximum and minimum values of floating potential. Maximum floating potential occurs when the powered electrode is at its most positive potential; minimum floating potential occurs when the powered electrode is at its most negative potential.

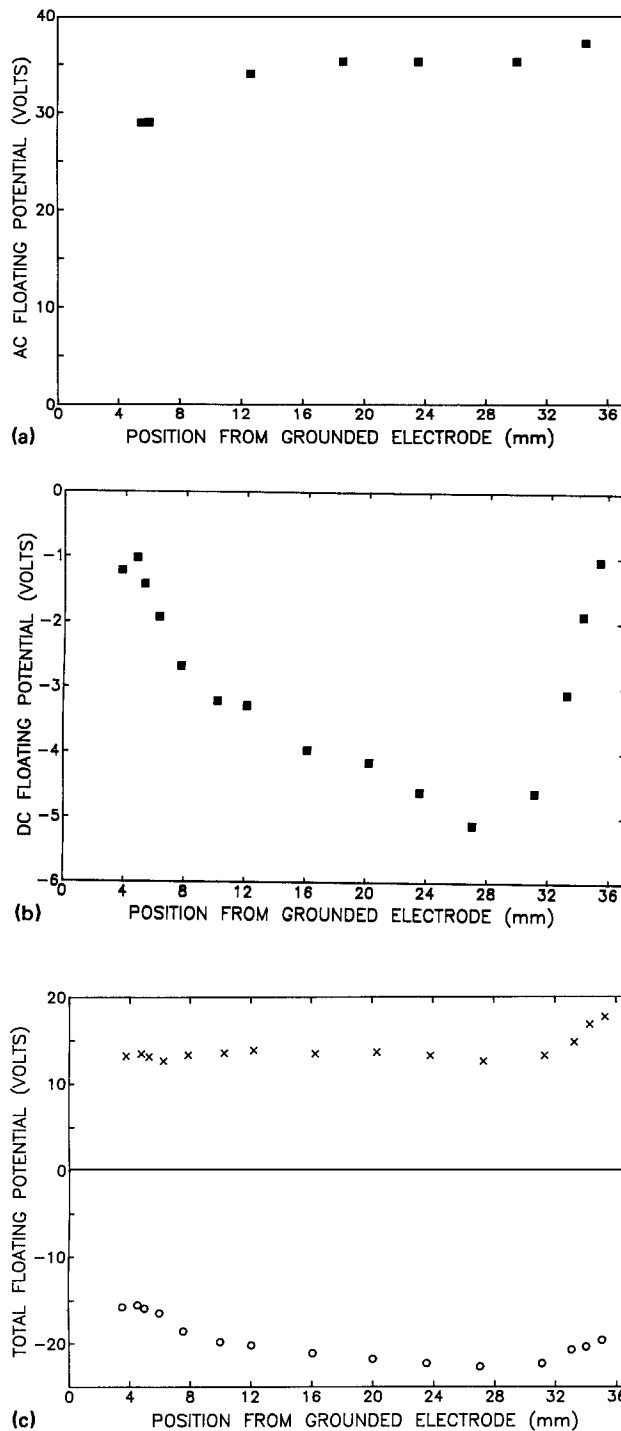


FIG. 3. Floating potential as a function of position across the discharge from the grounded electrode. (a) Peak-to-peak values of the sinusoidal ac signal. (b) dc magnitude of the time-averaged floating potential. (c) Total floating potential at its minimum (O) and maximum extent. The standard error in the data is smaller than the size of the data points.

Figure 4 shows the total electron current obtained 5 mm from the grounded electrode as a function of voltage on the probe tip at two times. The curve at lower voltage (open circles) corresponds to the plasma at its potential minima and the higher voltage curve (crosses) corresponds to the potential maxima of the plasma. Both curves (the extrema of the plasma) show two rapid rises in total electron current as

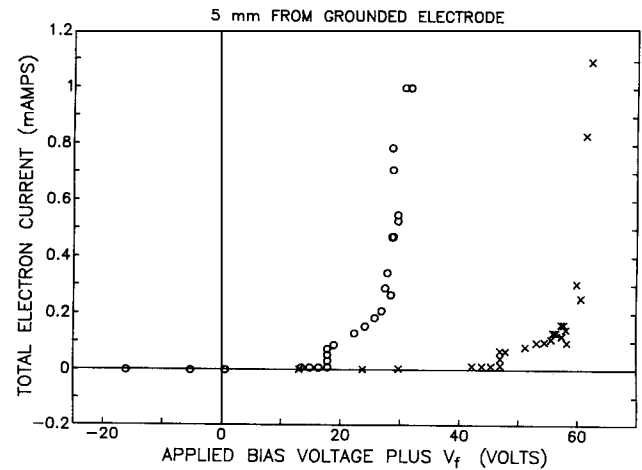


FIG. 4. Total electron current as a function of voltage on the probe tip at the plasma potential minima (O) and maxima (x) for a location close to the grounded electrode in the sheath region. Note the electron beam components at 18 and 48 V. The scatter in the data is indicative of its relative error.

the voltage on the probe tip is increased. The first of these steep current rises (occurring at 17 V for the minimum plasma potential curve and 47 V for the maximum potential curve) is due to an electron beam component in the plasma. The second steep rise (near 30 and 60 V) occurs at the plasma potential.

When the probes are moved to the center of the discharge, the number of mean-free paths between the electrode and probe are increased. The directed energy of the electron beam is degraded through collisions. Figure 5 shows the total electron current obtained 16 mm from the grounded electrode at the two extrema of the discharge. The two rises of

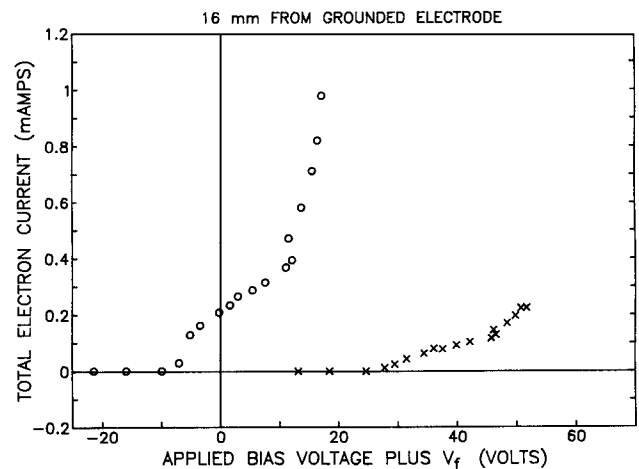


FIG. 5. Total electron current as a function of voltage on the probe tip at the plasma potential minima (O) and maxima (x) for a location near the center of the discharge. Note that the electron beam components are degraded. The scatter in the data is indicative of its relative error.

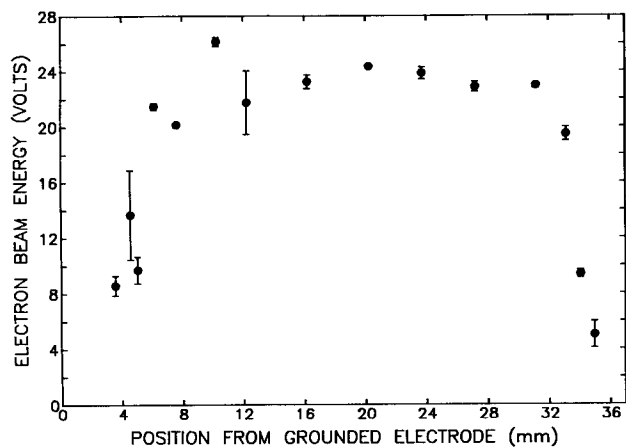


FIG. 6. Electron beam energy in electron volts as a function of the position from the grounded electrode at the plasma potential minima. Representative error bars are shown.

potential are still seen, but the shape is closer to that shown in Fig. 2(b), as expected. The energy of the electron beam component of the electron energy distribution can be determined from the separation of the onset of the current rise due to the beam component from the current rise due to plasma potential. Figure 6 shows the energy of the beam as a function of position across the discharge at the plasma potential minimum. The beam energy clearly follows the expected potential distribution. The energy is lower near the electrodes since the electrons have not yet experienced the full potential difference of the sheath. The beam energy taken from the plasma potential maximum curves shows a similar behavior. Error bars are shown on all data points.

A relative measure of the number of electrons in the beam component can be obtained by measuring the height of the electron current knee in the time-resolved electric probe

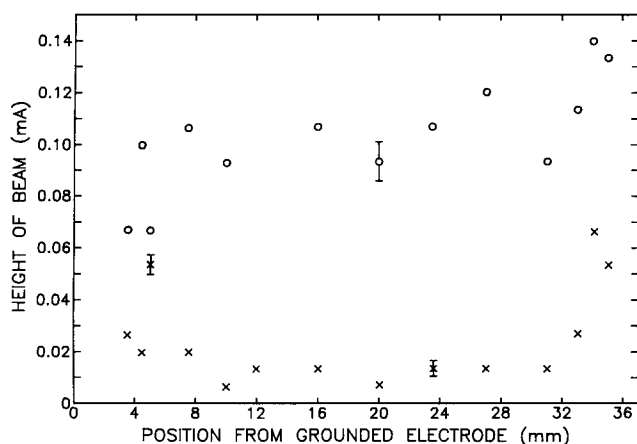


FIG. 7. Magnitude of the electron beam component as a function of position from the grounded electrode at the plasma potential minima (O) and maxima (x). Representative error bars are shown.

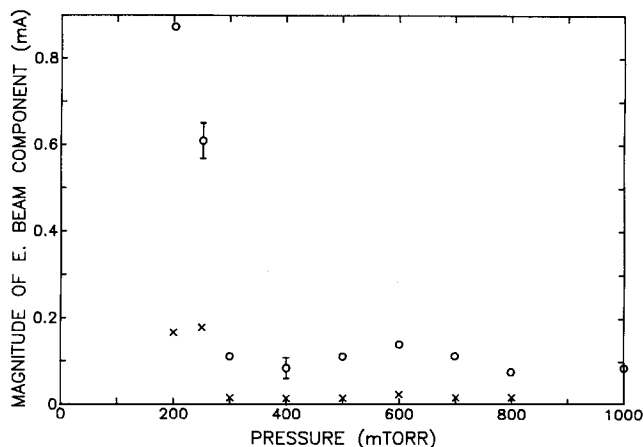


FIG. 8. Magnitude of the electron beam component as a function of discharge pressure 5 mm from the grounded electrode at the time of plasma potential maximum and minimum. Representative error bars are shown.

curves of Figs. 4 and 5. Figure 7 shows the height of this component in milliamperes as a function of position across the discharge at the two extrema of the plasma. In the plasma potential minima curve (crosses), the degradation of the electron beam is clearly seen as the electrons traverse the sheath and undergo more collisions. The curve for the plasma potential maxima shows a higher height of the beam component and degradation only when moving toward the center of the discharge from the powered electrode. Unfortunately the dependence as a function of position of the height of the beam component at the plasma potential maximum showed much scatter. There was a larger error inherent in determining the height of the knee on the maxima plasma potential $I-V$ curves than on the minimum plasma potential $I-V$ curves.

To ensure that the first sharp rise of the $I-V$ curves was indeed due to an electron beam and not enhanced ionization, the magnitude of the electron beam component 16 mm from the grounded electrode was measured as a function of pressure. Results at the plasma extrema are shown in Fig. 8. If the signal were due to enhanced ionization it would rise with pressure since the neutral density and hence the ionization rate near the probe tip would increase. The opposite trend is observed. The signal falls with increasing pressure due to a shorter mean-free path of the electrons and hence their shorter opportunity to be accelerated by the electric field in the sheath.

The potential distribution as a function of position at the time of maximum voltage on the powered electrode and minimum voltage on the powered electrode is shown in Fig. 9. The potentials on the powered electrode itself are inferred from the calibrated waveform sampler. The potential in the plasma are taken from the time-resolved $I-V$ characteristics. Error bars are shown for each point.

IV. DISCUSSION

When time-resolved Langmuir probe $I-V$ characteristics are obtained two steep rises in current at particular bias vol-

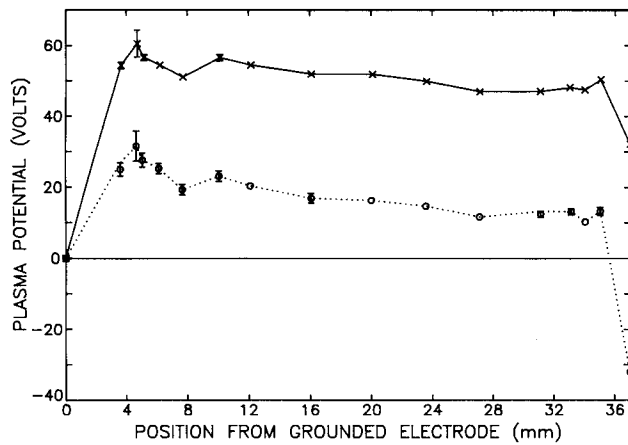


FIG. 9. Time-resolved potential variation across the discharge at the minimum (O) and maximum (X) points of the 13.56 MHz rf cycle. Error bars are shown for every point.

tages are clearly seen. The data in this paper shows that the first rise is due to an energetic electron beam component. The energy of this group of electrons clearly follows the potential distribution and the number of electrons in this group decrease as the number of electron-neutral collisions increase. This decrease in number can be accomplished by raising the neutral pressure (Fig. 8) or by probing further from the accelerating electric field of the sheath (Fig. 7).

If the first steep I - V rise were plasma potential and the second rise due to enhanced ionization, no variation in the voltage difference between the two knees would be seen as a function of position in the discharge. In addition, the signal from the second knee would increase with increasing pressure. This is not observed.

Due to this observed electron beam component of the electron energy distribution, predictions of plasma composition based on time-averaged Maxwellian electron energy distributions will be in error. Beam energies in excess of 10 eV (as reported here) can change ionization cross section by many orders of magnitude. Measurement of time-averaged quantities will miss this energetic electron component.

These experimental measurements agree with some recent theoretical models. Time-dependent electron energy distributions have shown beam components arising from acceleration in the sheath.¹² Work on plasma potential distribu-

tions^{13,14} show the sinusoidal variation and even the small dips in plasma potential observed just inside the sheath (at 8 and 34 mm in Fig. 9).

Future work will include measurements of the instantaneous electron energy distribution at the time when the powered electrode has a zero potential, ion energy analysis of the incident flux on the grounded electrode, and complete time-resolved measurements of a methane plasma. Direct comparison of experimental data to theoretical models is also planned.

ACKNOWLEDGMENTS

This work was supported by the NSF Presidential Young Investigator Award (NSF-CBT-84-51599) and donations of equipment from INTEL Corp. and Motorola Corp. We would like to thank the Plasma Science and Technology Division of the American Vacuum Society (AVS) for inviting this paper for presentation at the 36th National Symposium of the AVS.

- ¹ *Handbook of Plasma Processing Technology*, edited by S. M. Rossnagel, J. J. Cuomo, and W. D. Westwood (Noyes, Park Ridge, NJ, 1990).
- ² R. K. Janev, W. D. Langer, K. Evans, Jr., and D. E. Post, Jr., *Elementary Processes in Hydrogen-Helium Plasmas*, (Springer, Berlin, 1987).
- ³ J. B. O. Caughman II, D. N. Ruzic, and D. J. Hoffman, *J. Vac. Sci. Technol. A* **7**, 1092 (1989).
- ⁴ Jeffrey L. Wilson, J. B. O. Caughman II, Phi Long Nguyen, and D. N. Ruzic, *J. Vac. Sci. Technol. A* **7**, 972 (1989).
- ⁵ Jeffrey L. Wilson, Master's thesis, University of Illinois, 1989.
- ⁶ J. W. Swift and M. J. R. Schwar, *Electrical Probes for Plasma Diagnostics* (Hilff, London, 1970).
- ⁷ J. G. Laframboise, University of Toronto Institute of Aerospace Studies Report No. 100, 1966.
- ⁸ Francis F. Chen, University of California at Los Angeles, Dept. of Electrical Engineering (unpublished).
- ⁹ N. Benjamin, *Rev. Sci. Instrum.* **53**, 1541 (1982).
- ¹⁰ G. R. Misium, A. J. Lichtenberg, M. A. Lieberman, *J. Vac. Sci. Technol. A* **7**, 1007 (1989).
- ¹¹ N. Hershkowitz, in *Plasma Diagnostics*, edited by O. H. Auciello and D. L. Flamm (Academic, New York, 1989).
- ¹² M. J. Kushner, *Trans. Plasma Sci.* **PS-14**, 188 (1986).
- ¹³ G. R. Misium, *J. Vac. Sci. Technol. A* **8**, 1642 (1990).
- ¹⁴ R. W. Boswell and D. Vender, *J. Vac. Sci. Technol. A* (submitted).